International Symposium
On Turbulence and Shear Flow
Phenomena (TSFP-9)
June 30 - July 3, 2015 *Melbourne, Australia*

DRAG REDUCTION EFFECT DUE TO FINITE PERMEABLE WALL IN TURBULENT CHANNEL FLOW

Youhei Takagi
Department of Materials Engineering Science
Osaka University
1-3 Machikaneyama Toyonaka, Osaka 560-8531, Japan
takagi@cheng.es.osaka-u.ac.jp

Masayoshi Nakamoto
Department of Materials Engineering Science
Osaka University
1-3 Machikaneyama Toyonaka, Osaka 560-8531, Japan
m.nakamoto@cheng.es.osaka-u.ac.jp

Yasunori Okano
Department of Materials Engineering Science
Osaka University
1-3 Machikaneyama Toyonaka, Osaka 560-8531, Japan
okano@cheng.es.osaka-u.ac.jp

ABSTRACT

A three-dimensional numerical simulation for turbulent channel flow with permeable wall was carried out to investigate the dependency of permeable wall thickness on drag reduction. The permeability in the porous media attached on the outer solid wall was modelled with the Darcy-Forchheimer model, and the thickness of permeable wall was parametrically changed up to the ratio of 20% to the bulk fluid height. The governing equations for incompressible fluid in the both bulk fluid and permeable regions were discretized by the finite volume method and solved by the PISO algorithm.

When the thickness of permeable wall was comparable with that of the turbulent boundary layer, drag was reduced and its reduction ratio reached up to about 10%. When the sweep and ejection near wall was properly controlled due to the wall permeability, the vortex structure was stabilized and its formation process was not frequently repeated, therefore, turbulent drag reduction was achieved.

INTRODUCTION

Painting for ship hull is a basic technology for preventing biofouling in seawater, and various painting materials have been developed. Hydrogel painting forming hydrated layer in seawater has been developed by mimicking marine life's body surface such as dolphin. This new painting has only the function of antifouling but drag reduction effect that the maximum drag reduction ratio is about 10% in a field experiment (Yamamori and Shimada, 2009). Since hydrogel has cross-linked structure to capture water inside the network, swollen painting in seawater has a characteristic as permeable wall. Suga *et al.* (2011) carried out the PIV measurement for turbulent channel flow with porous plate wall and investigated the effect of fluid permeability on turbulent vortex structure. Direct numerical simulations for turbulent channel flow with permeable wall were also conducted (Hahn *et al.*, 2002; Breugem and Boersma, 2005), however, the permeable wall property related with hydrogel painting was hardly investigated. In this study, we carried out a turbulent channel flow simulation with finite permeable wall and discussed the dependency of permeability wall thickness on turbulent drag reduction.

NUMERICAL METHOD

Figure 1 shows the schematic of channel flow with finite permeable walls. The flow was bounded by finite permeable porous plate attached on outer solid wall and the periodic boundary conditions were adopted in the streamwise (x) and spanwise (z) directions. The thickness of porous plate δ_p was changed from the ratio of 1% to that of 20% for the bulk flow width δ_f as shown in Table 1. The domain sizes of the streamwise and spanwise directions were $4\pi\delta_f$ and $2\pi\delta_f$, respectively, and the grid numbers (N_x, N_y, N_z) were 149, 129-158, 129 in the x-, y-, z-directions, respectively. The Reynolds number based the bulk mean velocity and the total channel width including porous region was 5600. The governing equations were the following continuity and Navier-Stokes equations for incompressible fluid.

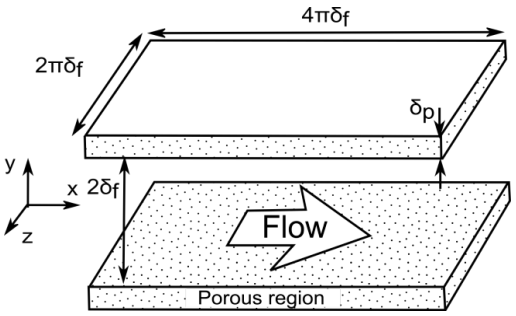

Fig. 1 Schematic of turbulent channel flow with permeable porous wall.

Table 1 Numerical condition.

Case	N_x, $N_y^f+N_y^p$, N_z	δ_p/δ_f
1%D	149, 129+8, 129	0.01
3%D	149, 129+20, 129	0.03
5%D	149, 129+29,129	0.05
10%D	149, 129+15, 129	0.10
20%D	149, 129+25, 129	0.20
Flat	149, 129, 129	-

$$\nabla \cdot \mathbf{u} = 0 \tag{1}$$

$$\frac{\partial \mathbf{u}}{\partial t} + \mathbf{u} \cdot \nabla \mathbf{u} = -\frac{1}{\rho}\nabla p + \nu \nabla^2 \mathbf{u} + (1-\varphi)\mathbf{F} \tag{2}$$

where **u** is velocity, and t time, and ρ density, and p pressure, and ν kinematic viscosity, and ϕ the porosity, and **F** the source term by calculating the following Darcy-Forchheimer equation:

$$\mathbf{F} = \nabla \frac{p}{\rho} = -\frac{\nu}{\sqrt{K}}\mathbf{u} - c_F \frac{c_F}{K} |\mathbf{u}|\mathbf{u} \tag{3}$$

where K is the permeability, and c_F the Forchheimer coefficient. The value of ϕ was 0.8 in the homogeneous porous region and the other values of porous parameter were K = 0.02 and c_F = 0.17 (Suga *et al*., 2011). On the other hand, in the bulk fluid region, the value of ϕ was zero and the source term was not considered. In order to maintain a constant flow rate, the pressure gradient term in the right-hand side of Eq. (2) was adjusted at each time step. The governing equations were discretized by the finite volume method and solved by the PISO algorithm. The numerical solution was obtained by the OpenFOAM.

RESULTS AND DISCUSSION

Friction coefficient C_f was calculated by using the FIK identify equation (Fukagata *et al*., 2002), and the drag reduction ratio (DR) to the drag of flat plate case was calculated as shown in Table 2. In the case of 20%D, the drag increased due to the large pressure loss in the porous region, however, in the cases of thin porous plate (3%D and 5%D), remarkable drag reductions up to 10.6% were achieved. The porous thickness normalized in wall unit δ_p^+ was 5 in the maximum drag reduced case and its value corresponded to the thickness of turbulent boundary layer. The thinnest porous case of 1%D had not drag reduction effect.

Table 2 Friction coefficient and drag reduction ratio.

Case	δ_p^+	C_f(x10^3)	DR[%]
1%D	2	7.31	-0.2
3%D	5	6.47	10.6
5%D	9	6.55	9.6
10%D	18	7.16	1.3
20%D	37	7.56	-4.3
Flat	-	7.25	-

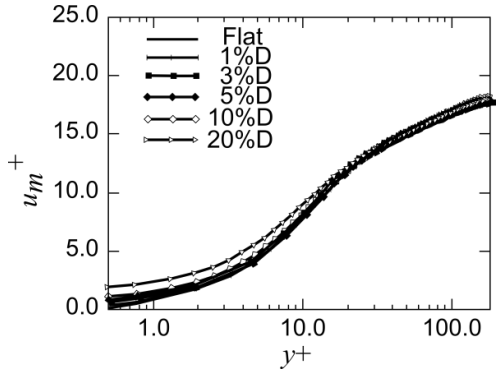

Fig. 2 Mean velocity profile.

The ensemble-averaged streamwise velocity in the wall-normal direction is shown in Fig. 2. At the boundary between the bulk flow and porous regions, non-zero velocity, that is, slip velocity occurred as same as hydrophobic wall turbulence. Although the slip velocity increased as the permeable wall thickness increased, the case of 20%D with the large slip velocity did not lead to drag reduction. Therefore, it was found that the drag reduction mechanism due to permeable wall was different from that of hydrophobic wall suggested by Min and Kim (2004). Figure 3 shows the r.m.s values of velocity fluctuation in each direction. When drag was reduced (3%D, 5%D, and 10%D), the peak values were smaller than that of Flat case, and turbulent flow was stabilized compared with the standard flat channel. On the other hand, at the drag-increased case (20%D), the peak value of $u_{\text{r.m.s.}}$ significantly increased and its position approached at the small distance compared with the Flat case. This result was agreed with the experimental result by Suga *et al*. (2011) that the blocking effect was weakened on the permeable wall. The large fluctuation regions of $w_{r.m.s.}$ were apart from the wall compared with the Flat case, it was expected that the turbulent structure and its formation process near the wall were changed.

One of the statistical values to measure the state of turbulent structure is the invariant of velocity gradient tensor. The second and third invariant, Q and R, are calculated as follows:

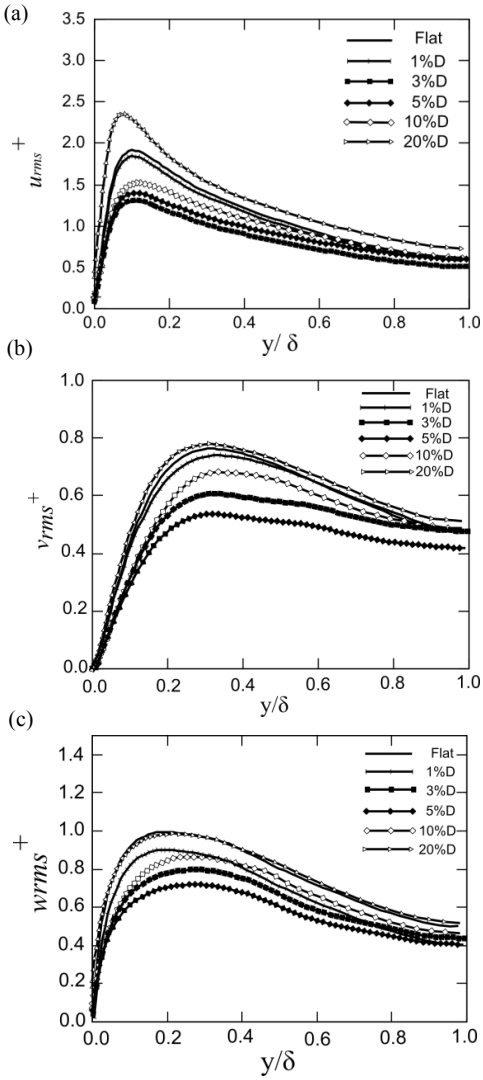

Fig. 3 The r.m.s value of velocity fluctuation: (a) streamwise, (b) wall-normal, and (c) spanwise components.

$$Q = \frac{1}{2}\left(S_{ij}S_{ji} + \Omega_{ij}\Omega_{ji}\right) \quad (4)$$

$$R = \frac{1}{3}\left(S_{ik}S_{kj}S_{ji} + 3\Omega_{ik}\Omega_{kj}S_{ji}\right) \quad (5)$$

where S_{ij} is the strain rate tensor and Ω_{ij} is the vorticity tensor. The Q value means the relative strength between vorticity and strain rate and the R value does the balance between strain rate production and vortex stretching. Figure 4 shows the joint probability density function of Q and R sampled on the x-z plane of $y^+ = 20$ for the drag-reduced case (3%D) and the drag-increased case (20%D). In the both cases, the probability distribution of Q was not much different, and the size and intensity of generated vortical structures were same magnitude. On the other hand, the distribution of R was different: the R value of the 3%D took almost zero and that of the 20%D was

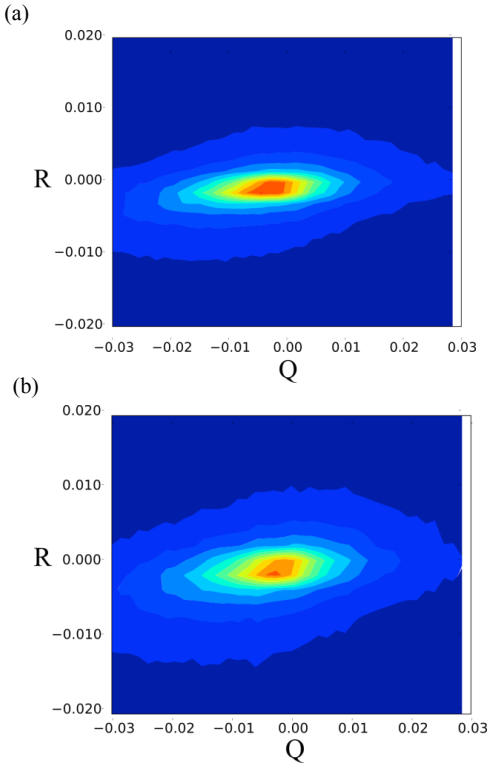

Fig. 4 Joint probability function of the second and third invariants of velocity gradient tensor for the sampling along y+ = 20: (a) 3%D, (b) 20%D.

distributed in the wide range. Since the large R value means the occurrence of vortex compression and stretching, the generated vortex structures were stable for the 3%D and unstable for the 20%D. The frequency of vortex generation/bursting cycle was enhanced/suppressed by the permeable wall property.

To discuss the relation between the permeability in porous plate and the drag reduction from the viewpoint of turbulent structure formation, we visualized the flow and vorticity fields near the wall. Figures 5 and 6 show the snapshots of velocity field and vortex structure in near the wall. In the flat plate case of Fig. 5, the strong longitudinal vortex pair with negative and positive streamwise vorticities was clearly seen and this coherent structure led to large energy dissipation, that is, turbulent drag. On the other hand, in the 3%D of Fig. 6, longitudinal vortices were weakened due to wall permeability. Since the penetrated fluid into porous region was bounded with the outer solid wall in a finite distance and returned to the bulk fluid region, the sweep and ejection that contributed the generation and bursting processes of longitudinal vortex were suppressed and the energy dissipation related with drag decreased. Although the laminarization of flow filed was not observed in the present simulation, the generated large-scale structure was stabilized compared with that of the flat plane channel as shown in the Q-R joint probability density function of Fig. 4.

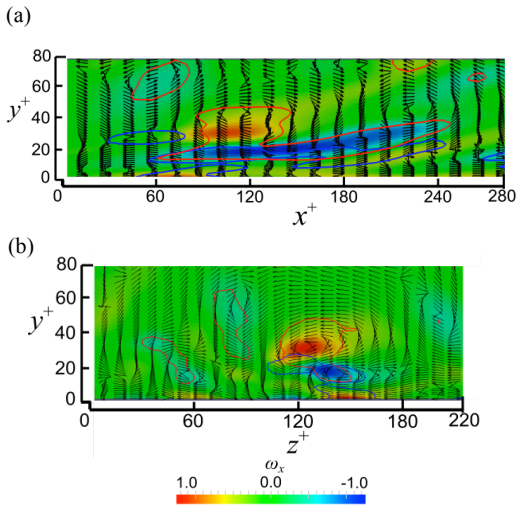

Fig. 5 Instantaneous flow field and vortex structure near the wall in the case of Flat: (a) in the *x*-*y* plane of $z^+ = 120$, (b) in the *y*-*z* plane of $x^+ = 120$. Vectors represent velocity fluctuation and the colour contour is the sreamwise component of vorticity. Red lines are the iso-lines of the positive second invariant of velocity gradient tensor, $Q+ = 0.2$ and blue lines the iso-lines of dissipation rate, $\varepsilon^+ = 2.8\times10^{-3}$.

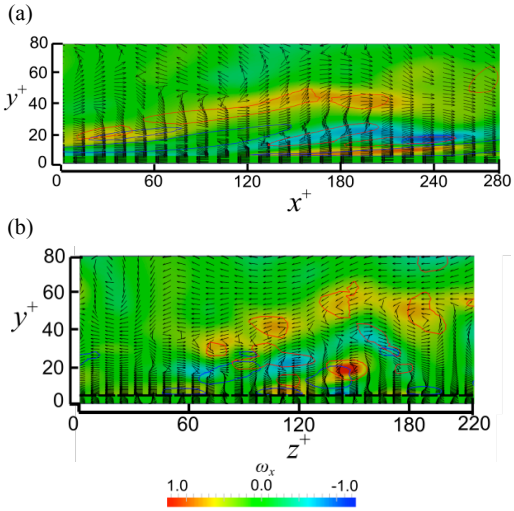

Fig. 6 Instantaneous flow field and vortex structure near the wall in the case of 3%D: (a) in the *x*-*y* plane of $z^+ = 120$, (b) in the *y*-*z* plane of $x^+ = 120$. The vectors, contours, and iso-lines are drawn as same as Fig. 5.

CONCLUSION

A three-dimensional simulation of turbulent channel flow with finite permeable wall was carried out and the relation between the fluid permeability and near-wall turbulent structure. As the thickness of permeable wall was increased, the slip velocity along the interface between the bulk fluid and permeable wall regions increased proportionally, however, the drag reduction was not linearly proportional to the thickness. When the thickness of porous plate was 3% to the channel width of bulk fluid region, the drag reduction ratio took the maximum value of 10.6%. At this case, since the fluid circulation between bulk fluid region and porous plate occurred, the coherent vortex structure elongated in the streamwise direction was stabilized and the energy dissipation was suppressed.

In future work, we will investigate the effect of pressure gradient variation on turbulent structure near the porous wall. Additionally, in order to consider the fluidity of hydrogel painting in water, we will introduce the viscoelastic model such as the Biot's theory (Biot, 1941).

REFERENCES

Biot, M. A., 1941, "General theory of three-dimensional consolidation", *J. Appl. Phys*., Vol. 12, pp. 155-164.

Breugem, W. P., and Boersma, B. J., 2005, "Direct numerical simulation of turbulent flow over a permeable wall using a direct and a continuum approach", *Phys. Fluids*, Vol. 17, 025103.

Fukagata, K., Iwamoto, K., and Kasagi, N., 2002, "Contribution of Reynolds stress distribution to the skin friction in wall-bounded flows", *Phys. Fluids*, Vol. 14, L73.

Hahn, S., Je, J., and Choi., H., 2002, "Direct numerical simulation of turbulent channel flow with permeable walls", *J. Fluid Mech.*, Vol. 490, pp. 259-285.

Min, T., and Kim, J., 2004, "Effects of hydrophobic surface on skin-friction drag", Phys. Fluids, Vol. 16, L55.

Suga, K., Mori, M., and M. Kaneda, 2011, "Vortex Structure of turbulence over permeable walls", *Int. J. Heat Fluid Flow*, Vol. 32, pp. 586-595.

Yamamori, N., and M. Shimada, 2009, "Verification of the reduction effect of new antifouling paint for ship bottoms "LF-Sea®" on the frictional resistance by utilizing actual ships", *TECHNO-COSMOS*, Vol. 22, pp. 28-33, in Japanese.